

Static and flowing regions in granular collapses down channels

Gert Lube

Research Division "Dynamics of the Ocean Floor," IFM-GEOMAR, Leibniz Institute for Marine Sciences, Wischhofstrasse 1-3, D-24148 Kiel, Germany

Herbert E. Huppert^{a)}

Institute of Theoretical Geophysics, Department of Applied Mathematics and Theoretical Physics, Centre of Mathematical Sciences, University of Cambridge, Wilberforce Road, Cambridge CB3 0WA, United Kingdom

R. Stephen J. Sparks

Centre of Environmental and Geophysical Flows, Department of Earth Sciences, Bristol University, Bristol BS8 1RJ, United Kingdom

Armin Freundt

Research Division "Dynamics of the Ocean Floor," IFM-GEOMAR, Leibniz Institute for Marine Sciences, Wischhofstrasse 1-3, D-24148 Kiel, Germany

(Received 15 November 2005; accepted 9 January 2007; published online 20 April 2007)

Through laboratory experiments we investigate inertial granular flows created by the instantaneous release of particulate columns into wide, rectangular channels. These flows are characterized by their unsteady motion, large changes of the free surface with time, and the propagation towards the free surface of an internal interface separating static and flowing regions. We present data for the time-dependent geometry of the internal interface and the upper, free surface for aspect ratios, a , in the range from 3 to 9.5 (where $a = h_i/d_i$ is the ratio of the initial height to basal width of the column). The data were analyzed by two different approaches. First, by integrating under the entire internal interface we obtained data for the static area, A_D , as a function of time for different a . Second, in order to characterize vertical deposition rates, we measured the thicknesses of the flowing region, $h_F(x, t)$, and the static region, $h_D(x, t)$, at fixed horizontal positions, x , and time, t , since the initiation of the experiment. We also determined detailed velocity profiles with depth at distances scaled to the final maximum runout distance to analyze the kinematic behavior of the flowing layer. In the initial free-fall phase, the temporal variation of the static area is independent of h_i and scales as $gd_i t$. During the subsequent lateral spreading phase, $A_D(t)$ varies linearly with time and the nondimensional deposition rate $(dA_D/dt)/(gd_i^3)^{1/2}$ is a linear function of a . The thickness of the interface $h_D(x, t)$ at constant x depends on a and varies linearly with time. The local deposition rate $\partial h_D/\partial t$ is not constant along the flow length. Data show that for the major part of the flow length $\partial^2 h_D/\partial t \partial x$ is constant. In the lateral spreading phase, the velocity profiles are characteristically linear with a basal exponential region, a few grains in thickness, which separates static from moving regions. The shear rate is a constant dependent on a modified initial height \tilde{h}_i as $(g/\tilde{h}_i)^{1/2}$, where \tilde{h}_i is a characteristic length scale in the system describing the fraction of the granular column actually involved in the flowing region. © 2007 American Institute of Physics. [DOI: 10.1063/1.2712431]

I. INTRODUCTION

The complex physical behavior of granular media is of great interest in diverse areas including agriculture, chemical engineering, fundamental physics, the pharmaceutical industry, and the Earth sciences. Understanding the physics of dense, granular flows is of particular importance in understanding the propagation of geophysical mass flows and how to predict their runout. Examples of such flows include highly destructive pyroclastic flows formed in explosive volcanic eruptions and avalanches of debris or snow. Numerical simulations of geophysical mass flows over natural terrain are being used more frequently by geologists and geophysicists to produce hazard maps for volcanic¹ and mountainous

areas.² Despite many fundamental studies dedicated to the dynamics of dense granular flows, these simulations have to circumvent the problem that the underlying constitutive equations are still unknown. The general approach has been to derive depth-averaged equations for steady flow conditions and introduce empirical friction laws to try to obtain agreement between data and experiments.³⁻⁷ For the case of free-surface flows driven by gravity, three major flow geometries have been studied extensively: chute flows on rough inclines at angles slightly above the static angle of repose, rotating drums, and heap flows. A review of the rheological models obtained in these steady flow situations was recently presented in the collective paper by G.D.R. Midi.⁸

Recently, free-surface flows of granular media have been investigated in a fourth type of flow geometry by laboratory experiments⁹⁻¹⁴ and by computer simulations.¹⁵⁻¹⁷ These

^{a)}Electronic mail: heh1@esc.cam.ac.uk

studies all consider the fundamental problem of the collapse of an initially static granular column released instantaneously onto a rough horizontal bed. Granular collapse flows differ considerably from thin, quasisteady granular chute flows at inclines slightly above the static angle of repose referenced above. The main differences are that they are unsteady and involve large changes of the free surface with time as well as the propagation towards the free surface of an internal interface separating static and flowing particles.

Here we present detailed experimental results on the dynamics of the internal interface and the dynamic and kinematic behavior of the overlying particle flow. This work develops further our studies of column collapses in axisymmetric^{9,10} and two-dimensional geometries,¹¹ which we now briefly summarize. In axisymmetric geometry, we considered the unhindered spreading of initially cylindrical columns of heights h_i and radii r_i . In the two-dimensional geometry, the granular regions had initial height, h_i , basal length, d_i , and were released into long channels of different but large width. In both geometries, we employed a wide range of particle sizes, shapes, and densities and varied the floor roughness systematically from smooth to rough. The major governing parameter is the initial aspect ratio, a , in axisymmetric geometry defined as the ratio h_i/r_i and in two-dimensional geometry as h_i/d_i . Maximum runout distances, r_∞ and d_∞ , in axisymmetric and two-dimensional geometries, respectively, the maximum deposit height at the origin, h_∞ , and the time, t_∞ , to reach the final runout, were found to be independent of the different grain types and the roughness of the base. The axisymmetric experiments focused on the final geometry and propagation of the flow front with time. Our study of two-dimensional granular collapses included the observation of the internal deformation, the dynamics of the free surface, and the interface between the static and the flowing layer.

These experiments allowed investigation of the three major stages describing the collapse. In the first stage, the collapse is controlled by the free-fall behavior of the column. The upper part of the column, above a critical height of approximately $2.8d_i$, is in purely vertical motion (in two dimensions). Once the top of the column has reached this critical height, the second phase of collapse is dominated by lateral motion, which ceases abruptly at t_∞ , when the interface between static and flowing particles has reached the free upper surface. In these first two phases, the influence of the bounding walls is very small, as indicated by (horizontal) plug flow velocity profiles across the free surface with minor shear at the walls and strong slip. There is a (quite different) third phase of motion, which involves thin and slow avalanching across the free surface to stabilize the steep central part of the pile. In this phase, frictional effects of individual particles between each other and with the bounding walls become strong. The form of collapse, its duration and the shape of the final deposit are effectively controlled by the physics of the flowing layer and the propagation of the separating interface towards the free surface.

The plan of the paper is as follows: In Sec. II, we explain the experimental setup and the techniques that were used to determine the velocity profiles in the flowing layer and the

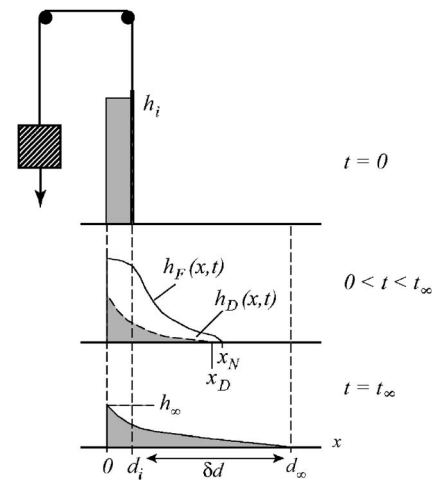


FIG. 1. Experimental setup with a sketch of the initial column, the interface between a lower static layer (gray) and an upper flowing layer (white); and the final deposit.

geometry of the free surface and the interface. An analysis of the spatial and temporal evolution of the free surface and the interface is presented in Sec. III. Data of the velocity profiles in the flowing layer is presented in Sec. IV. A summary of our results and further discussion are presented in Sec. V.

II. METHODS

The experiments investigate two-dimensional granular flows formed by the collapse of rectangular columns of sand into a wide horizontal channel. We employed the same experimental setup described in Ref. 11 (Fig. 1). A container accommodated the granular material at one end of the tank. A rectangular box of the same width, 20 cm, as the channel and variable initial basal length d_i included a frontal gate to release the granular material. A release mechanism was constructed to allow for very fast and reproducible lifting velocities of the gate. It consisted of releasing a large weight connected to the gate via a pulley construction at the ceiling. The weight fell freely for the first 0.75 m to reach a high velocity (approximately 4 m s^{-1}) before it lifted the gate extremely rapidly. The time for the gate release in any experiment ($\sim 0.1 \text{ s}$) was much less than the typical time scale of the resulting motion ($\sim 1 \text{ s}$). We employed a mixture of industrial black and light gray colored quartz sands of grain-size $1.4 \pm 0.4 \text{ mm}$. This was found to give the best contrast results for the digital image analysis described below. In this study, the initial aspect ratio a was varied systematically from 3 to 9.5 by using two different values of d_i (6 cm and 9 cm) and different masses of sand.

Each experiment was conducted twice. In the first run, the entire flow was filmed through the transparent frontal pane. Before preparing the initial columns of sand, a 5 mm grid was tied to the inner side of the frontal pane to give a reference frame and a fast camera at 120 frames/s then recorded the experiment. The flows were captured and analyzed digitally. At every fifth frame (at intervals of $\sim 0.04 \text{ s}$), we mapped the free surface to obtain $h_F(x,t)$ (Fig. 1). To obtain curves of the interface between static and flowing par-

ticles, $h_D(x,t)$, we first analyzed every fifth and sixth frame using the Pattern Match algorithm of Dalziel.¹⁸ Finally, we carefully corrected, where necessary, these curves to exactly match the interface between the uppermost static and the lowermost flowing particle. In the second run, we positioned the camera as close as possible and perpendicular to the frontal plane at a distance $\delta d/3+d_i$, where δd is the difference between the maximum runout distance, d_∞ , and the initial width d_i (Fig. 1). We could thus obtain very detailed high-speed movies for the analysis of the velocity profile with depth, again using the 5 mm grid as a reference.

III. EVOLUTION OF THE INTERFACE AND FREE SURFACE

A. Spatial evolution: Qualitative observations

We first contrast the temporal evolution of the free surface, the interface and the depth of the flowing layer for a typical experiment [Figs. 2(a), 2(b), and 3(c)]. The inset in Fig. 2(b) shows the length of the interface, L_D , determined from appropriately integrating $h_D(x,t)$ as a function of time. A detailed description of the evolution of the free surface as a function of the aspect ratio is given in Ref. 11. Figure 2(a) illustrates the two subsequent phases of collapse. The first phase is dominated by the free fall of the column, and the top of the column remains nearly undisturbed. In this free fall phase, the point of maximum height of the flowing layer remains at an approximately constant distance d_i from the y axis [Fig. 2(c)]. In the second, lateral spreading phase, deformation occurs along the entire free surface [Fig. 2(a)]. The point of maximum height of the flow propagates outwards with time [Fig. 2(c)]. As the flowing layer increases in length, its maximum thickness reduces until the flowing layer has reached an approximately constant thickness (except for the origin and at the front where it goes to zero). As shown previously in Refs. 11, 13, and 14, at the beginning of the experiment the internal interface appears as a straight line intersecting at a zero height at $x=d_i$, where x is the distance from the origin. This initial line is inclined at approximately 60° to the horizontal. Throughout the entire experiment, the internal interface propagates upwards towards the free surface [Fig. 2(b)], and the static area increases with time. In the lateral spreading phase, L_D also varies approximately linearly with time [inset Fig. 2(b)]. Results similar to those presented in Fig. 2 for $a=7$ were obtained for all tested values of the aspect ratio.

B. Static versus flowing material

Column collapses can be geometrically described by the two time-dependent functions $h_F(x,t)$ and $h_D(x,t)$. Plots similar to Fig. 2(b) can be used to determine the area of static material, A_D , defined by

$$A_D(t) = \int_{x=0}^{x=x_D(t)} h_D(x,t) dx, \quad (1)$$

where $x_D(t)$ is the horizontal coordinate of the front of the deposited layer. The data so obtained are plotted as A_D-A_W against time in Fig. 3, where $A_W=0.5d_i^2 \tan 60^\circ$ is the area of

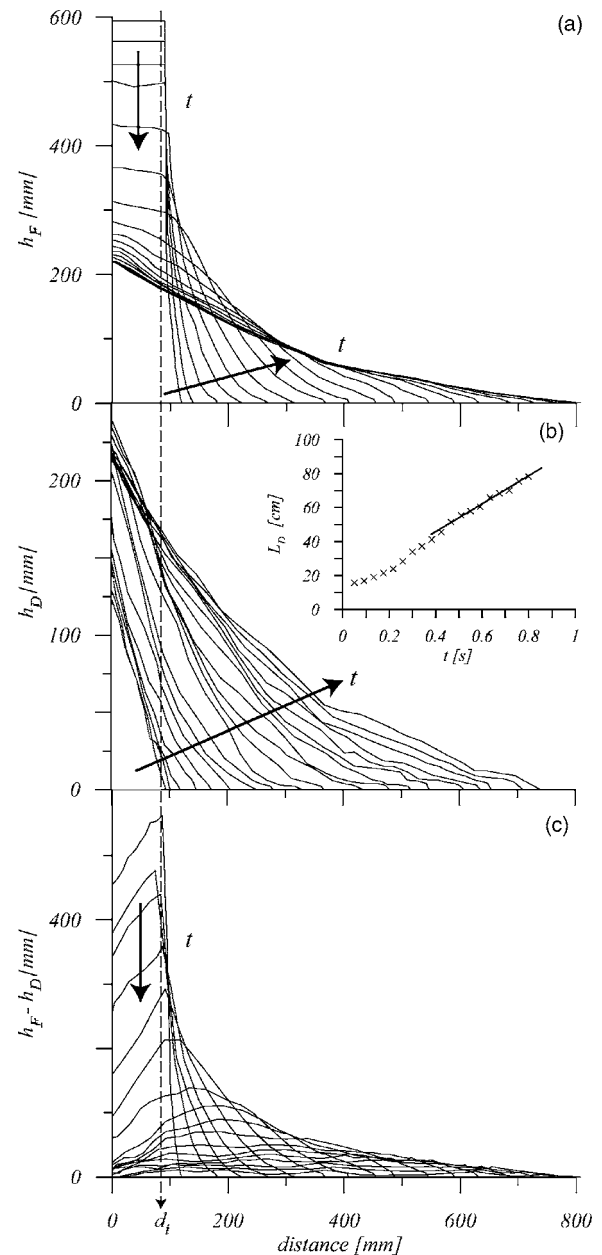


FIG. 2. An example of the evolution of: (a) the free surface; (b) the internal interface; and (c) the thickness of the flowing layer with time, at constant time intervals of 0.416 s for an experiment where $a=7$ and $d_i=9.05$ cm. Note the different scale of the y axis in (b) chosen for a clearer illustration. Inset shows the temporal variation of the length of the interface, L_D . The gray triangle drawn in (b) marks the static wedge formed in the beginning of the experiment.

the initial static wedge, and hence the initial value of A_D . Two different phases can be recognized. Without any normalization, the curves of A_D-A_W against time for different values of a collapse onto a universal curve in the first phase of collapse, where A_D-A_W is proportional to $gd_i^2 t^2$. There is a departure from this universal curve at a time dependent on a . In the lateral spreading phase, the static area increases linearly with time. Deposition rates dA_D/dt vary from 390 to 940 cm^2/s for $d_i=9.05$ cm and $a=3.4$ to $a=9$, respectively. By dimensional analysis we can express the deposition rate as

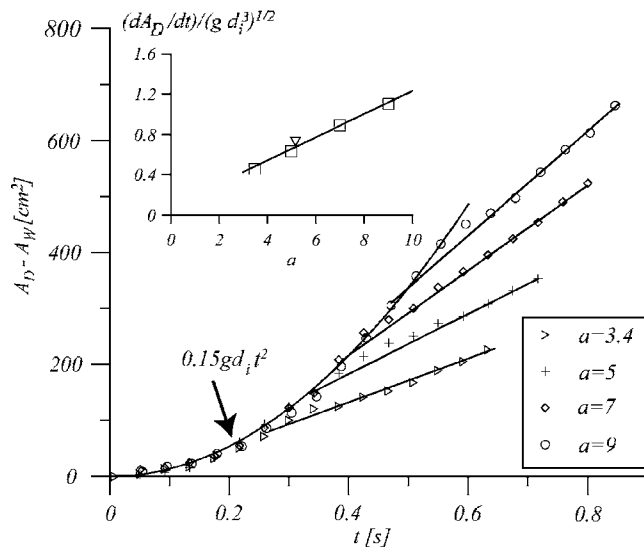


FIG. 3. The area of the static layer against time for different values of the aspect ratio and $d_i=9.05$ cm. There is a collapse of the data in the first phase to the function $A_D - A_W = 0.15gd_i t^2$. Linear functions and corresponding slopes drawn to data points in the lateral spreading phase illustrate the constant global deposition rates dA_D/dt for different aspect ratios. Inset shows data of the nondimensional deposition rate $(dA_D/dt)/(gd_i^3)^{1/2}$ against a for $d_i=9.05$ cm (\square) and $d_i=6.05$ cm (∇), and the linear best fit through the data.

$$dA_D/dt = (gd_i^3)^{1/2} f(a), \quad (2)$$

for some dimensionless function f of the aspect ratio. The inset in Fig. 3, where the deposition rate is plotted against $a(gd_i^3)^{1/2}$, shows that $f(a)$ is linear.

C. Vertical motion of boundaries

Figure 4 shows the temporal evolution of the thickness of the static layer, $h_D(x, t)$, at different horizontal distances x for a representative experiment where $a=5$ and $d_i=9.05$ cm. At $x=12$ cm and $x=22$ cm, the data h_D against time are well represented by two linear segments and a short, nonlinear, transitional region in between. The initial linear part is observed during the free-fall phase, whereas the final linear segment occurs during the lateral spreading phase. At the

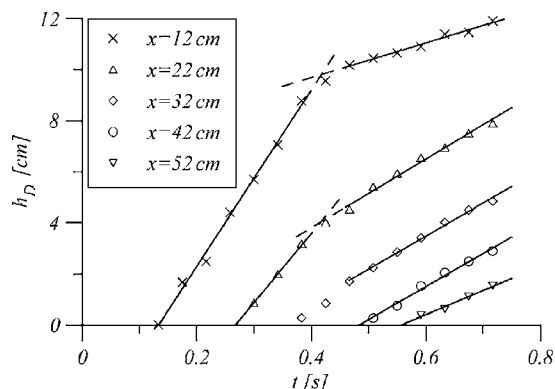


FIG. 4. The temporal variation of the thickness of the static layer, h_D , at different horizontal distances, x , for an experiment where $a=5$ and $d_i=9.05$ cm. There are two linear regions, representing the free-fall and lateral spreading phase, respectively, and a short transitional region in between.

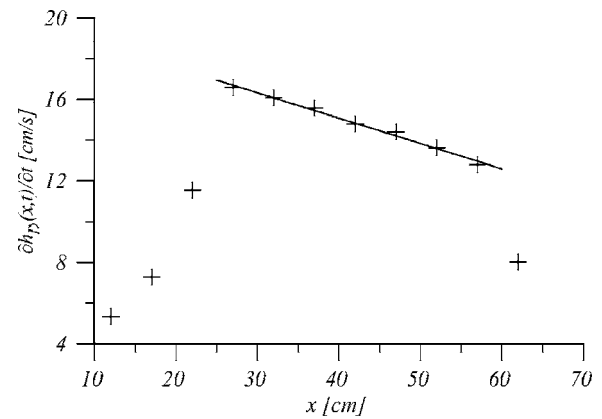


FIG. 5. The variation of the local deposition rate, $\partial h_D(x, t)/\partial t$ in the lateral spreading phase as a function of the horizontal distance, x , for an experiment where $a=7$. Deposition rates were determined as the slope from best-fit linear regressions to the data $\partial h_D(x)$ against time in the lateral spreading phase.

outer horizontal positions ($x=32$, 42 , and 52 cm), there is only one behavior corresponding to linear growth of the layer during the lateral spreading phase. The data show that during the lateral spreading phase there is a linear growth with time of the static layer along the flow length. However, $\partial h_D/\partial t$ is not constant along the flowing layer, but varies slightly with the horizontal distance, x . For the lateral spreading phase, where the variation of h_D with time is linear, we can calculate local horizontal deposition rates $\partial h_D(x, t)/\partial t$ by linear best fits. Figure 5 shows a graph of the local deposition rate as a function of x for an experiment where $a=7$. It is seen that, except close to $x=0$ and $x=d_\infty$, the deposition rate declines slightly in linear fashion during the spreading phase.

Without a general dynamical model for the internal interface and the free surface, we investigate the vertical variation of h_F and h_D at scaled horizontal distances only. We derive the scaling relationships for $h_D(t)$, $h_F(t)$, and $h_F(t) - h_D(t)$ at a fixed horizontal distance $\delta d/3 + d_i$. We choose this representative distance to be far from both $x=0$ and $x=d_\infty$, where either vertical or horizontal motions dominate, respectively. The flow front reaches this distance at constant fractions of the final time, t_∞ for different values of a .¹¹ Figure 6 shows the temporal evolution of h_D , h_F , and $h_F - h_D$ for different values of a and $d_i=9.05$ cm. After the flow front reaches the observation point, the thickness of the static layer, h_D , increases approximately linearly with time. The (near constant) local deposition rate, $\partial h_D/\partial t$, at $\delta d/3 + d_i$ increases with increasing aspect ratio. The local flow height, h_F , first increases before equilibrating at a final height, dependent on a . The thickness of the flowing layer, $h_F - h_D$, increases with time towards a maximum before decreasing to zero.

Figure 7 presents the same thickness data plotted against the nondimensional time, t/t_∞ , where t_∞ is the final emplacement time. The flow front and the internal interface arrive subsequently at constant fractions of the nondimensional time at the scaled horizontal distance $\delta d/3 + d_i$ ($\sim 0.4 t_\infty$ and $\sim 0.5 t_\infty$, respectively). Growth of the static layer thus starts a

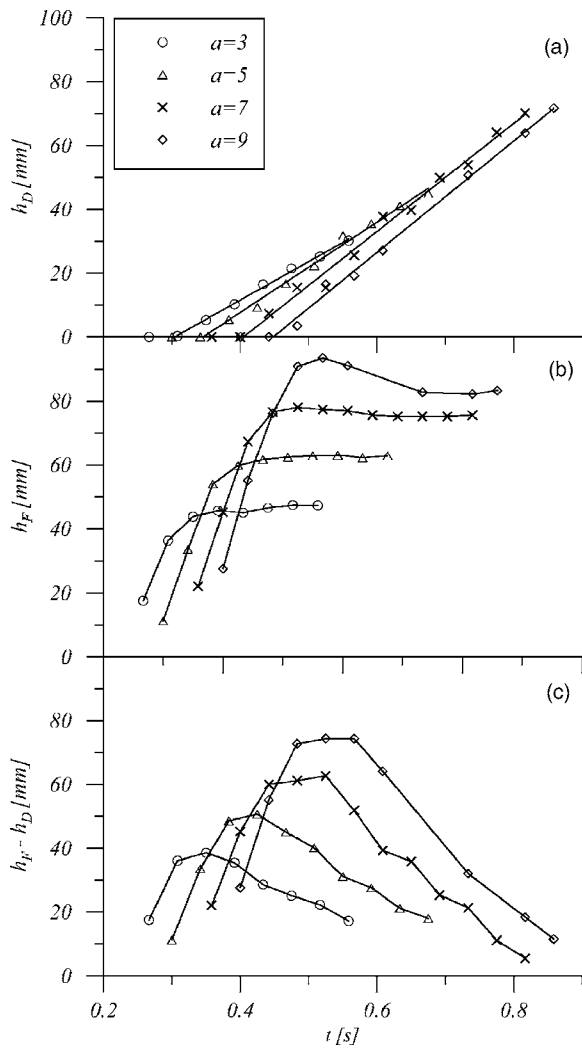


FIG. 6. Variation of: (a) the thickness of the static layer; (b) the free surface height; and (c) the thickness of the flowing layer, with time at a fixed position $\delta d/3+d_i$ for different values of a .

little time after the flow front has passed the location. The initial height, h_i , might be a relevant length to scale all the curves $h_D(t)$, $h_F(t)$ and $h_F(t) - h_D(t)$ in order to obtain universal curves for the data. However, using this scaling neither the time nor length scale would depend on the initial width of the column, d_i . Indeed, no collapses are obtained for non-dimensional groupings of h_D/h_i , h_F/h_i or $[h_F(t) - h_D]/h_i$ against non-dimensional time. By dimensional analysis the local deposition rate $\partial h_D(\delta d/3 + d_i, t)/\partial t$ can be expressed as a function of external parameters as

$$\partial h_D(\delta d/3 + d_i, t)/\partial t = (gd_i)^{1/2} H(a), \quad (3)$$

where H is a dimensionless function of the aspect ratio. From the experimental data of h_D against time we can calculate the local deposition rate by linear best fits. Figure 8 shows the non-dimensional local deposition rate $[\partial h_D(\delta d/3 + d_i, t)/\partial t]/[gd_i]^{1/2}$ plotted against the aspect ratio. The data for experiments with different values of the initial height, h_i , and the initial basal length, d_i , collapse onto a universal function $H(a)$ which is linear.

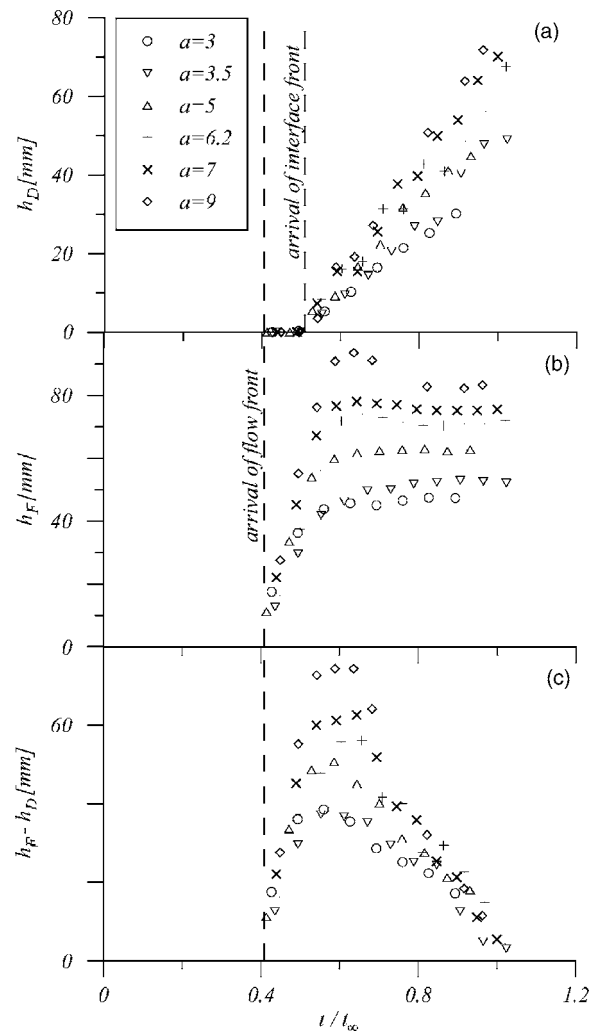


FIG. 7. The thickness of the static layer, h_D , the free surface height, h_F , and the thickness of the flowing layer, $h_F - h_D$, against non-dimensional time at the fixed position $\delta d/3 + d_i$.

We now develop a Lagrangian view of this problem. As shown in Ref. 11, the propagation of the flow front with time in two dimensions is self-similar; and all columns for $a > 2.8$ relax towards self-similar profiles. Therefore, self-

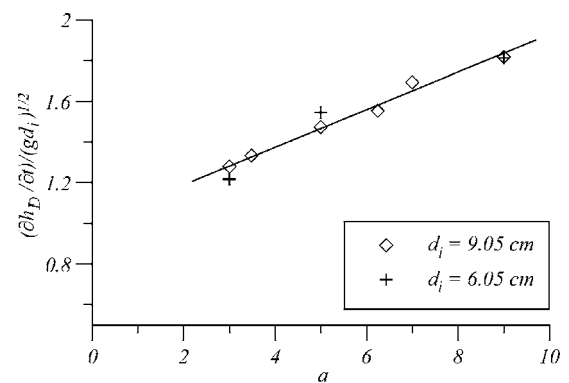


FIG. 8. The non-dimensional local deposition rate against the aspect ratio at the fixed position $\delta d/3 + d_i$ for $d_i = 9.05$ cm (\diamond) and $d_i = 6.05$ cm ($+$), and a linear best fit through the data. Deposition rates were determined as the slope from best fit linear regressions to the data $\partial h_D(\delta d/3 + d_i)$ against time in the lateral spreading phase.

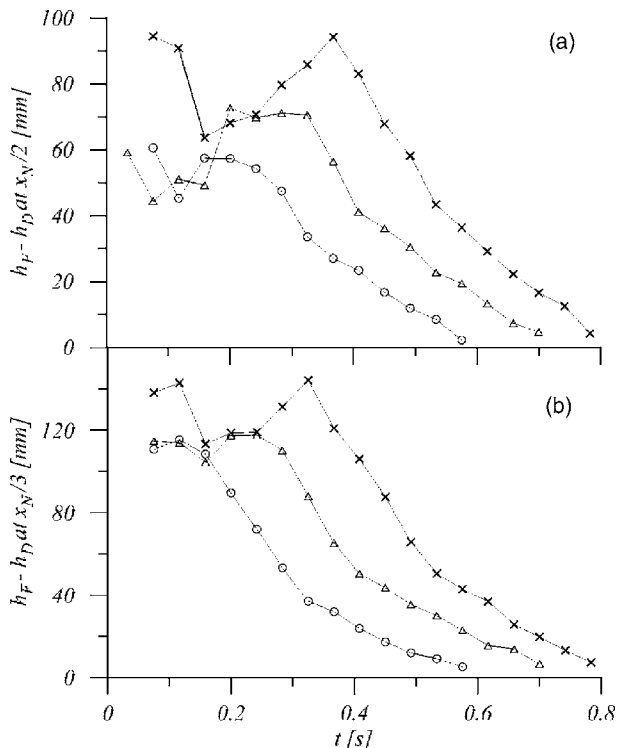


FIG. 9. The depth of the flowing layer at a scaled distance $x_N(t)/n$ with (a) $n=2$ and (b) $n=3$ for $a=3.4, 5,$ and 7 . Same symbols as in Figs. 6 and 7.

similarity of the curves $h_F(x,t)$ and $h_D(x,t)$ might be expected. From our experimental data we obtained $h_F(x,t)$ and $h_D(x,t)$ at constant fractions of the instantaneous flow front position $x_N(t)$. Figure 9 shows the temporal evolution of the depth of the flowing layer for three values of a at the time-dependent distance $x_N(t)/n$ [with $n=2$ in Fig. 9(a) and $n=3$ in Fig. 9(b)]. The first part of the curves, which relates to the initial free-fall phase, shows a decreasing region followed by an increasing region. There is a final continuously decreasing part constituting the lateral spreading phase. In Fig. 10 we plot the same data in nondimensional form, using the length scale h_i and the experimentally determined final time, t_∞ , as the length scale to determine the function M defined by

$$(h_F - h_D)/h_i = M(t/t_\infty). \tag{4}$$

A very good collapse is obtained for all tested values of h_i after approximately $0.4-0.5 t_\infty$ in the spreading phase. We have also tested other values of n ($0.6 \leq n \leq 10$), which also result in a collapse of the data $(h_F - h_D)/h_i$ against nondimensional time during the lateral spreading phase. The different curves $M(t/t_\infty, n)$ merge as $t/t_\infty \rightarrow 1$, illustrating the experimental observation that, towards the end, the thickness of the flowing layer is approximately constant along the flow length.

IV. VELOCITY PROFILES IN THE FLOWING LAYER

The velocity profiles in the flowing layer vary in both space and time. In the initial free-fall phase, all particles above a critical height, $h_c \sim 2.8 d_i$, are in purely vertical motion. In the flow front region in direct contact with the base, a strong parabolic profile with a plug-like top and a high slip

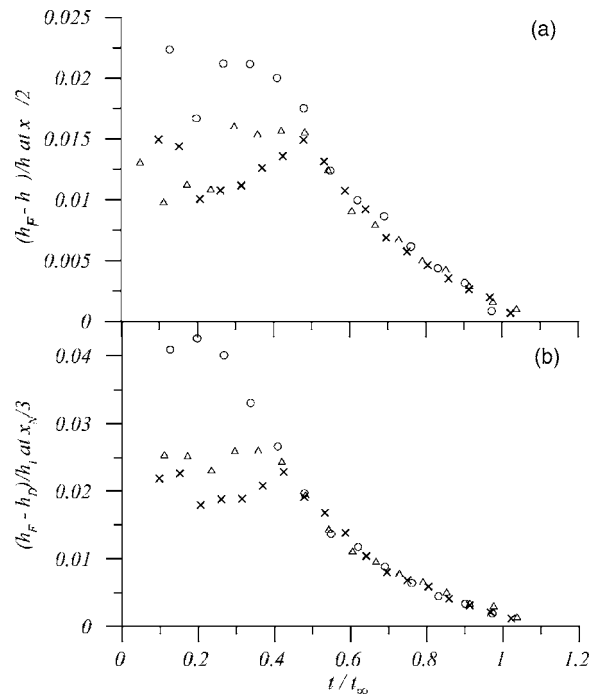


FIG. 10. The nondimensional depth of the flowing layer at a scaled distance $x_N(t)/n$ with (a) $n=2$ and (b) $n=3$. Same symbols as in Figs. 6 and 7.

velocity at the base exists.¹¹ During the entire experiment, close to $x=0$ or $x=x_N$, the profiles tend to purely vertical or horizontal motion, respectively. In the second, lateral spreading phase, except close to the origin and the flow front, the velocity profiles show the typical form illustrated in Fig. 11. From the internal interface upwards, we distinguish between two transient regions: a lower exponential part and an upper linear part. At the very top of the flowing layer, there is a thin region of roughly constant thickness (approximately 3 par-

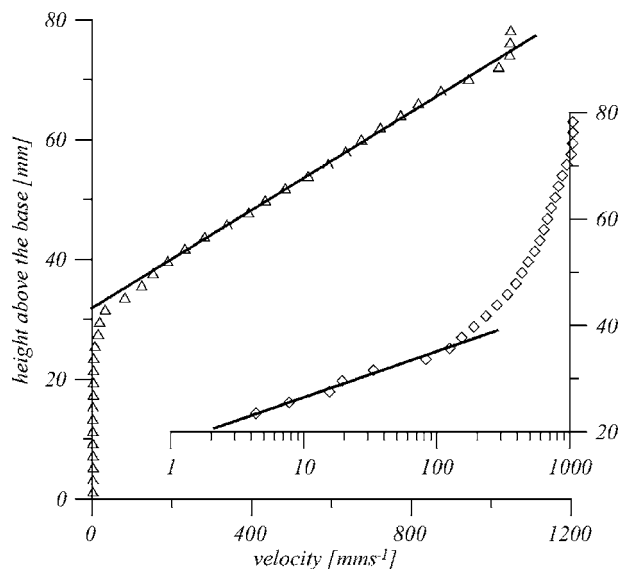


FIG. 11. Example of the typical form of velocity profile in the lateral spreading phase, including the static layer, a lower exponential region, an upper linear section and an upper plug-like region restricted to a few grains. Inset shows the same data in a linear-log plot to highlight the exponential region.

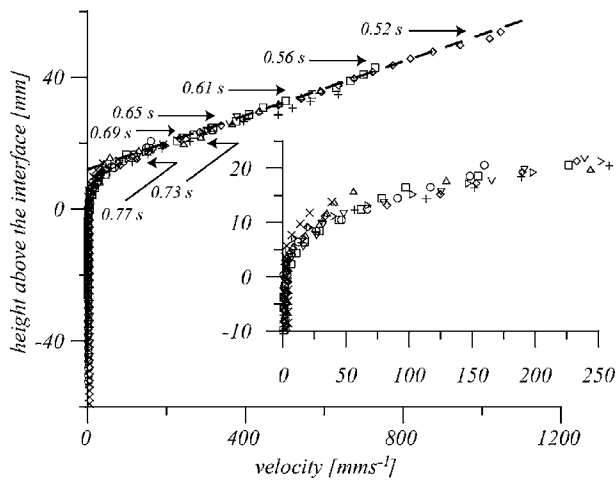


FIG. 12. Collapse of all velocity profiles for an experiment where $a=7$ after the development of the interface at $\delta d/3+d_i$. Different symbols represent the velocity profiles at different times in the interval $0.5 t_\infty < t < t_\infty$. The arrows and corresponding times mark the instantaneous position of the upper free surface. Inset highlights the region close to the interface.

ticle diameters) deviating from the major, linear part. The region with the largest change in velocity and depth with time is the linear part of the profile. The typical form of the velocity profiles during the lateral spreading phase has been previously reported in Refs. 11 and 13. Velocity profiles similar to that described here are also typical for heap flow and rotating drum geometries under steady flow conditions.^{8,19} A common characteristic of all three geometries is the existence of an internal interface separating static and flowing regions of granular material.

PIV analysis on high-speed movies of our second experimental series allows us to obtain detailed velocity profiles with depth at scaled distances $\delta d/3+d_i$. For each aspect ratio, a universal curve $h-h_D$ against velocity exists that collapses all profiles obtained after the arrival of the interface front at times $t > 0.5 t_\infty$. Figure 12 illustrates the collapse for an experiment with $a=7$ and times $0.5 t_\infty < t < t_\infty$. The lower exponential part remains constant in form and thickness (approximately 8–10 particle diameters), whereas the thickness of the linear part decreases with decreasing thickness of the flowing layer. Collapsed velocity profiles similar to that presented in Fig. 12 for $a=7$ are obtained for all values of a . We can characterize these profiles by expressing a shear rate γ as the inverse slope of a best linear fit through the linear part of the velocity field. By dimensional arguments this shear rate can be written as

$$\gamma = (g/\tilde{h}_i)^{1/2} F[a = h_i/d_i, \phi/h_i], \quad (5)$$

where ϕ is the particle diameter. We introduce here the modified initial height, \tilde{h}_i , defined by

$$\tilde{h}_i = h_i - d_i \tan(60^\circ)/2 \quad (6)$$

as a length scale that describes the fraction of the granular column actually involved in the flowing region. When we plot the experimentally determined shear rates for all values of h_i and d_i against the shear rate scale $(g/\tilde{h}_i)^{1/2}$ (Fig. 13), the data collapse onto the linear function

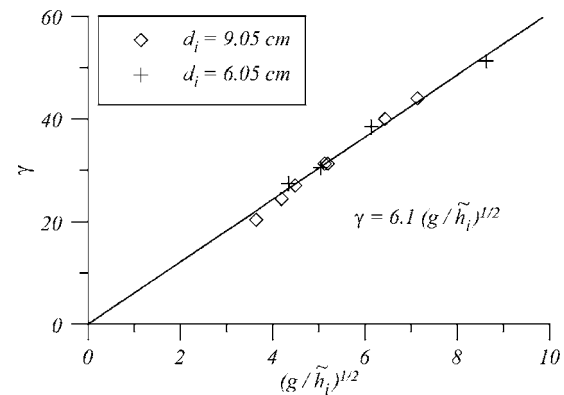


FIG. 13. The shear rate obtained from best linear fits of the linear part of the velocity profiles plotted against $(g/\tilde{h}_i)^{1/2}$, where \tilde{h}_i is the modified initial height (see text for details).

$$\gamma = 6.1 (g/\tilde{h}_i)^{1/2}. \quad (7)$$

We note that, if instead of \tilde{h}_i the initial height h_i is used in the term for the shear rate scale, the data collapse onto a linear function that gives physically unrealistic negative values for large values of h_i . Since the ratio ϕ/h_i is very small in comparison to the aspect ratio, we may define a nondimensional shear rate

$$\gamma(\tilde{h}_i/g)^{1/2} = F(a). \quad (8)$$

Figure 14 shows that $F(a)$ is effectively constant.

In contrast to the clear dependence of the shear rate on the aspect ratio (or on \tilde{h}_i) that we have demonstrated here, a different behavior is claimed in Ref. 13. These authors follow a similar scaling approach as proposed for steady uniform flows observed in heap flow and rotating drum geometries (e.g., Refs. 8 and 19). They suggest that velocity profiles obtained for different values of a , at different times and for different particle diameters, ϕ , collapse onto a universal curve by normalizing the velocity by $(g\phi)^{1/2}$ and depth by ϕ . With a linear fit through the linear part of all the normalized profiles, the authors of Ref. 13 claim the relationship $\gamma = 0.3(g/\phi)^{1/2}$. We think that their interpretation of the data is misleading and substantiate our view by the following

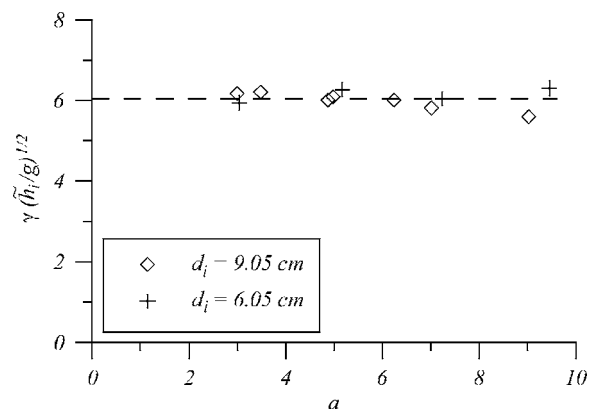


FIG. 14. The nondimensional shear rate $\gamma(\tilde{h}_i/g)^{1/2}$ plotted against the aspect ratio.

arguments. First, in their presented data, the systematic variation of the velocity profiles as a function of time is not shown. Instead particular profiles for experiments with different a and ϕ were depicted. Second, the presented velocity profiles nearly exclusively correspond to the late stages of the experiment (i.e., when the thickness of the flowing layer is less than 7–8 particle diameters). Thus, a dominant part of the considered profiles correspond to the lower exponential region, and the linear part of the presented profiles has a depth of hardly five particle diameters. Finally, the presented data show a large scatter around the proposed linear function $\gamma=0.3(g/\phi)^{1/2}$. This large scatter (particularly that in the exponential region), however, gives reason to assume that the form and/or depth of the lower exponential region is dependent upon particle characteristics. This view and suggestions for further investigations of this problem are amplified in the last section.

V. SUMMARY AND DISCUSSION

This paper presents experimental results of the dynamics of static and moving regions of granular material that characterize inertial granular flows initiated by column collapse. During collapse, the upper flowing region continuously deposits material from its base. Thus, the area of static material grows with time, and the internal interface separating upper, flowing and lower, static material propagates towards the free surface.

The discrete nature of the internal interface allowed us to quantify its temporal and spatial variation as a function of the initial aspect ratio. The resulting data were analyzed by two different approaches. First by integrating under the entire interface we determined global deposition rates, dA_D/dt . Second we measured the thickness variation of the flowing and static regions at fixed horizontal distances, x , and were able to calculate local deposition rates, $\partial h_D(x,t)/\partial t$. At a fixed position, scaled to the final maximum runout, we also analyzed the form and temporal variation of the velocity profile with depth in the flowing layer.

Experimental observations in previous studies (referenced in Sec. I) have shown qualitatively that inertial granular column collapses involve two transient stages: an initial free-fall phase and a subsequent lateral spreading phase. These two phases are also evident in the contrasting behavior of the motion of the interface, and consequently in the rate of deposition which occurs from the base of the flowing layer.

In the free-fall phase, the rate of growth of the static area with time is independent of the initial height and scales as $gd_i t$. This finding is in good agreement with previous results which show that, in this initial phase, also the shape of the free surface below the critical height $h_c \sim 2.8 d_i$ (including the horizontal position of the flow front) does not change with h_i .^{11,16}

In the lateral spreading phase, the static area increases linearly with time dependent on the aspect ratio. Granular columns with higher aspect ratios show higher deposition rates, and the nondimensional deposition rate $(dA_D/dt)/(gd_i^3)^{1/2}$ is a linear function of the aspect ratio. The local vertical growth of the interface is independent of the

local flow depth and velocity. Data show that, for the major part of the flow length, the derivative $\partial^2 h_D/\partial t \partial x$ is a constant dependent on the aspect ratio, but experimental runs with two connected high-resolution, high-speed cameras are needed to explore this relationship in detail. This is planned in future investigations.

Our data of the vertical velocity profiles with depth show: (a) a time-invariant form comprising a lower exponential and an upper linear region; and (b) a scaling relationship for the shear rate as $\gamma=c(g/\tilde{h}_i)^{1/2}$. The shear rate is, however, independent of the local flow depth and velocity, but decreases by increasing the area involved in the flow (i.e., increasing a). Beside column collapses, granular flows in heap flow and rotating drum geometries comprise linear vertical velocity profiles. However, no physical explanation for this has yet been offered. This behavior is in contrast with steady uniform flows on inclines close to the (static) angle of repose. In this situation, the shear rate varying as the square root of depth results in the so-called Bagnold scaling. The widely accepted reason for this scaling relationship is the constant ratio of shear stress and normal stress.²⁰

Here we interpret the characteristics of the velocity profiles in a qualitative way and suggest some directions for future investigations. One possible way of looking at the problem is by a simple rheological analog. Viscous fluids produce a classic parabolic profile with shear rate increasing linearly with depth. If one could describe inertial granular flows by a rheological law, then this would have to involve a linear dependence of “effective” viscosity with depth. This law implies the effects of viscosity are zero (or very small) near the free surface and increase linearly with depth.

Whereas the velocity of the interface and the major (linear) part of the velocity profile are time-invariant, the lower exponential region seems to have the key role in describing how particles at the base of the flowing layer come to rest. We propose here that within this region, the flow velocity decreases below a critical threshold, which causes a rapid decline in granular temperature and an increase in interparticle friction. Taking a typical speed of 10 cm/s and thickness of 0.5 cm for the exponential region gives a time scale of 0.05 s. It might be worthwhile testing through molecular dynamics simulation, for example, whether this time scale is relevant in describing how an agitated particulate system becomes motionless when external forcing is removed. The data presented in Ref. 13 for different grain diameters give reason to assume that form and/or depth of the exponential region may vary with the particle characteristics. Detailed investigations making use of a high resolution, high-speed camera of the exponential region for flows where the grain diameter is varied by at least an order of magnitude will provide further insight. Moreover, it will be most interesting to investigate the dynamics of the interface for collapses in inclined channels, in particular approaching the static angle of repose (AOR). When the basal inclination is equal to the AOR, the interface may coincide with the rigid base. To further stress this idea, at inclination sufficiently above the

AOR, even downward motion of the interface into loose bed material could be expected, giving a framework to describe both sedimentation and erosion from granular flows.

ACKNOWLEDGMENTS

We would like to thank Lydie Staron, John Hinch, and Dominique Vella for insightful discussions. For the construction of the experimental setup and data acquisition the help Sebastian Muenn and Stefan Schulze was invaluable. G.L. is grateful for the support of a David Crighton Fellowship awarded by the University of Cambridge. This study was supported by the Deutsche Forschungsgemeinschaft (Grant No. Fr 947/9-2). H.E.H. and R.S.J.S. acknowledge Royal Society Wolfson merit awards.

- ¹R. S. J. Sparks and W. P. Aspinall, "Volcanic activity: Frontiers and challenges in forecasting, prediction, and risk assessment," *AGU Geophysical Monograph "State of the Planet" 150, IUGG Monograph*, Vol. 19, pp. 359–374 (2004).
- ²S. Margreth, L. Stoffel, and C. Wilhelm, "Winter opening of high alpine pass roads: Analysis and case studies from the Swiss Alps," *Cold Regions Sci. Technol.* **37**, 467 (2003).
- ³S. B. Savage and K. Hutter, "The motion of a finite mass of granular material down a rough incline," *J. Fluid Mech.* **199**, 177 (1989).
- ⁴K. G. Anderson and R. Jackson, "A comparison of the solutions of some proposed equations of motion of granular materials for fully developed flow down inclined planes," *J. Fluid Mech.* **92**, 145 (1992).
- ⁵S. B. Savage, "Analyses for slow quasistatic high concentration flows of granular materials," *J. Fluid Mech.* **377**, 1 (1998).

- ⁶O. Pouliquen, "Scaling laws in granular flows down rough inclined planes," *Phys. Fluids* **11**, 542 (1999).
- ⁷R. M. Iverson and R. P. Denlinger, "Flow of variably fluidized granular masses across three-dimensional terrain. Part I: Coulomb mixture theory," *J. Geophys. Res.* **106**, 537 (2001).
- ⁸G. D. R. Midi, "On dense granular flows," *Eur. Phys. J. E* **14**, 341 (2004).
- ⁹H. E. Huppert, M. A. Hallworth, G. Lube, and R. S. J. Sparks, "Granular column collapses," *Bull. Am. Phys. Soc.* **48**, 68 (2003).
- ¹⁰G. Lube, H. E. Huppert, R. S. J. Sparks, and M. A. Hallworth, "Axisymmetric collapses of granular columns," *J. Fluid Mech.* **508**, 175 (2004).
- ¹¹G. Lube, H. E. Huppert, R. S. J. Sparks, and A. Freundt, "Collapses of two-dimensional granular columns," *Phys. Rev. E* **72**, 041301 (2005).
- ¹²E. Lajeunesse, A. Mangeney-Castelnau, and J. P. Vilotte, "Spreading of a granular mass on a horizontal plane," *Phys. Fluids* **16**, 2371 (2004).
- ¹³E. Lajeunesse, J. B. Monnier, and G. M. Homsy, "Granular slumping on a horizontal surface," *Phys. Fluids* **17**, 103302 (2005).
- ¹⁴N. J. Balmforth and R. R. Kerswell, "Granular collapse in two dimensions," *J. Fluid Mech.* **538**, 399 (2005).
- ¹⁵R. R. Kerswell, "Dam break with Coulomb friction: A model for granular slumping?" *Phys. Fluids* **17**, 057101 (2005).
- ¹⁶L. Staron and E. J. Hinch, "Study of the collapse of granular columns using DEM numerical simulation," *J. Fluid Mech.* **545**, 1 (2005).
- ¹⁷R. Zenit, "Computer simulations of the collapse of a granular column," *Phys. Fluids* **17**, 031703 (2005).
- ¹⁸S. B. Dalziel, *DigiFlow User Guide*, <http://www.damtp.cam.ac.uk/lab/digiflow/> (2005).
- ¹⁹D. Bonamy, F. Daviaud, and L. Laurent, "Experimental study of granular surface flows via a fast camera: A continuous description," *Phys. Fluids* **14**, 1666 (2002).
- ²⁰O. Pouliquen, C. Cassar, Y. Forterre, P. Jop, and M. Nicolas, "How do grains flow: Towards a simple rheology of dense granular flows," *Proceedings Powders and Grains* (Stuttgart, 2005).